DOI 10.5162/SMSI2025/P49

Modeling of High-Sensitivity SAW Magnetic Field Sensors with Au-SiO_2 Phononic Crystals

Mohsen Samadi[1,*], *Jana Marie Meyer*[2], *Fabian Lofink*[2,3], *Martina Gerken*[1]
[1]*Integrated Systems and Photonics, Department of Electrical and Information Engineering, Kiel University, Germany*
[2]*Fraunhofer Institute for Silicon Technology ISIT, Itzehoe, Germany*
[3]*Microsystem Materials, Department of Materials Science, Kiel University, Germany*
[*]*mosa@tf.uni-kiel.de*

Summary:
In this study, we present a highly-sensitive SAW magnetic field sensor that utilizes phononic crystal structures with Au pillars embedded in a SiO_2 guiding layer. The sensor's sensitivity is considerably improved due to increased interactions between the SAW and the magnetostrictive material, facilitated by resonance effects within the PnC structure. Our proposed sensor thus demonstrates significantly enhanced performance compared to sensors with continuous delay lines.

Keywords: magnetic field sensor, magnetostriction, phononic crystal, surface acoustic wave

Introduction

Magnetic field sensors are crucial in various applications for accurate measurement and detection of magnetic fields [1-4]. Surface acoustic wave (SAW) based magnetic field sensors have been exploited to detect minute changes in magnetic fields by utilizing the ΔE effect, where the Young's modulus of magnetostrictive materials changes under an external magnetic field, causing phase modulation of the SAW [5-8]. This modulation is detected and measured, providing information about the magnetic field strength. Phononic crystals (PnC), i.e., engineered materials with periodic arrangements, allow precise control over acoustic wave propagation and dispersion [9-15]. Integrating PnC structures into SAW magnetic field sensors enhances sensitivity and performance, promising advancements for applications that require accurate magnetic field detection [16].

Here, we model a SAW magnetic field sensor with a PnC structure embedded within the guiding layer. The proposed sensor is schematically illustrated in Fig. 1. A thick silicon substrate is coated by a 1 µm-thick $Al_{0.77}Sc_{0.23}N$ piezoelectric layer [17]. Two gold IDTs are devised on the surface of the AlScN layer to generate and detect a Rayleigh wave at a center frequency of approximately 250 MHz. A 2D square lattice of Au pillars is embedded within the SiO_2 guiding layer between the two IDTs. These pillars are of the same thickness as the guiding layer (h_p = h_{GL} = 4.5 µm). The entire PnC structure is then coated by a continuous FeCoSiB layer with a thickness of h_{MS} = 200 nm.

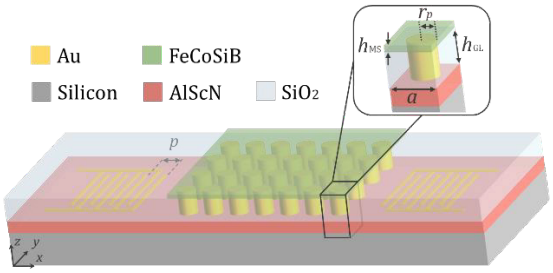

Fig. 1. SAW magnetic field sensor with Au-SiO_2 PnC. A magnified view of a unit cell of the PnC is shown with further details. a and r_p denote the lattice constant and the radius of the pillars, respectively. h_{GL} and h_{MS} represent the thicknesses of the guiding layer and the magnetostrictive layer.

Theoretical Model

To analyze the sensor's performance, we solve a set of coupled differential equations using the finite element method (FEM) [18,19]. For simplicity, we consider an isotropic magnetostrictive material whose mechanical stiffness tensor is determined by the Young's modulus (E) and Poisson's ratio (v).

Applying a magnetic field induces changes in the Young's modulus of the magnetostrictive material, denoted as the ΔE effect. The final value of the Young's modulus (E_f) is achieved by the superposition of the purely mechanical component (E_0) and the magnetically-induced component (ΔE) [20]. When accounting for a hard axis magnetization process:

$$E_f = \begin{cases} \left(\frac{1}{E_0} + \frac{1}{\Delta E}\right)^{-1} & |\mathrm{H}| < \mathrm{H}_K \\ E_0 & |\mathrm{H}| > \mathrm{H}_K \end{cases} \qquad (4)$$

Here, H_K denotes the effective anisotropy field and the magnetically-induced change in the Young's modulus (ΔE) can be obtained using the following formula:

$$\frac{1}{\Delta E} = \frac{9}{4}\frac{\mu_0 \lambda_S^2 \mathrm{H}^2}{K^2}\chi \qquad (5)$$

where μ_0, λ_s, and K are the magnetic vacuum permeability, the saturation magnetostriction, and the first-order anisotropy constant, respectively. Further details regarding the theoretical model and material parameters can be found in [16].

Results

We employed the finite element method (FEM) to calculate the band structure of the PnC and conducted a series of parameter sweeps using COMSOL Multiphysics to determine the optimal dimensions of the PnC for precise frequency matching between one of the PnC resonant modes with the center frequency of the Rayleigh mode generated by the IDT, i.e., *f*=250 MHz. The details of the simulation model can be found elsewhere [16]. Fig. 2(a) presents the band diagram calculated in Γ-X direction for a PnC with *a* = 5.6 µm and r_p = 0.25×*a* = 1.4 µm. The PnC dimensions are adjusted so that the second Rayleigh mode (R2) meets the frequency matching condition near the edge of the first Brillouin zone. In this region, formation of flat bands results in slower wave propagation for frequencies close to the band edges.

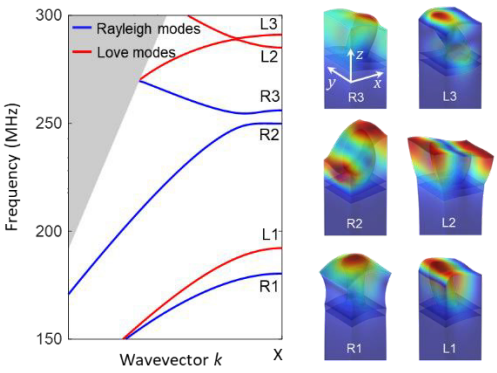

Fig. 2. Left: Band diagram of the PnC with a = 5.6 µm, r_p = 1.4 µm and h_p = 4.5 µm, calculated in the Γ-X direction of the first Brillouin zone. Rayleigh and Love modes are indicated by blue and red lines, respectively. The grey-shaded area outlines the sound cone. Right: Displacement profiles of the first three Rayleigh and Love modes calculated at the point X of the first Brillouin zone.

To investigate the sensitivity of our sensor, we subjected it to an external magnetic field in the range of $0.6\mathrm{H}_K < |\mathrm{H}| < 0.7\mathrm{H}_K$. Alteration of the magnetic field within this range induces a linear change in the Young's modulus of the FeCoSiB layer, ranging from 120 GPa to 115 GPa. This leads to a change in the SAW velocity and a phase shift in the output signal, which is analyzed to quantify the magnetic field strength.

The structural sensitivity of the sensor is defined as the change in the SAW phase velocity per unit change in the Young's modulus of FeCoSiB ($S_{str} = \partial v/\partial E_f$). Fig. 3(a) presents the band diagram of the second Rayleigh mode (R2 in Fig. 2) for two different Young's modulus values of 115 and 120 GPa. At the frequency of *f*=250 MHz, the phase velocity of the Rayleigh wave changes by Δ*v*~88 m/s, yielding a structural sensitivity of S_{str}~17.6 $\frac{m/s}{GPa}$. The Rayleigh mode propagating through the unpatterned guiding layer exhibits a phase velocity change of Δ*v*~7.5 m/s in response to the same variation in the Young's modulus of FeCoSiB, resulting in a structural sensitivity of S_{str}~1.5 $\frac{m/s}{GPa}$ (Fig. 3(b)).

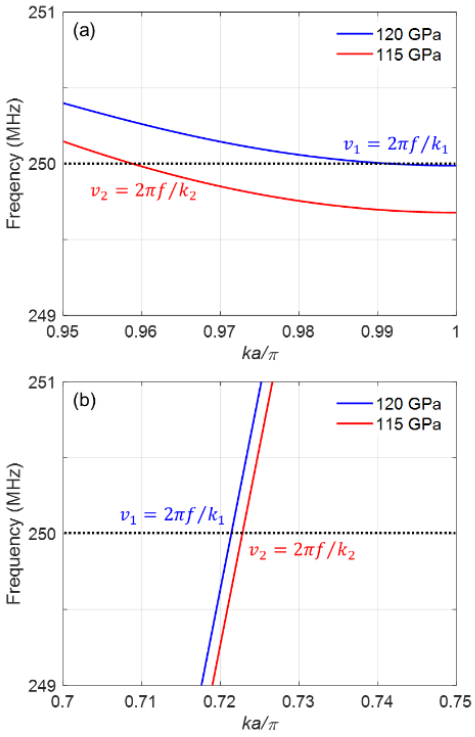

Fig. 3. Band diagrams of (a) the second Rayleigh mode of the PnC (R2 in Fig. 2) and (b) the Rayleigh mode propagating through the unpatterned guiding layer for the Young's modulus values of 120 and 115 GPa. v_1 and v_2 denote the phase velocity values acquired for 120 and 115 GPa, respectively.

The significant enhancement in the sensitivity of the SAW magnetic field sensor is attributed to resonance effects within the PnC structure. These effects cause the SAW to propagate through the PnC with an effectively lower velocity, resulting in an effectively increased interaction between the SAW and the magnetostrictive material, thereby improving the sensing capability of our sensor.

Acknowledgment

This work was funded by the German Research Foundation (Deutsche Forschungsgemeinschaft) via the collaborative research center CRC 1261 “Magnetoelectric Sensors: From Composite Materials to Biomagnetic Diagnostics”.

References

[1] J. Zhai, Z. Xing, S. Dong, J. Li, and D. Viehland, “Detection of pico-Tesla magnetic fields using magneto-electric sensors at room temperature,” *Appl Phys Lett*, vol. 88, no. 6, p. 62510, Feb. 2006.

[2] S. Zuo *et al.*, “Ultrasensitive Magnetoelectric Sensing System for Pico-Tesla MagnetoMyoGraphy,” *IEEE Trans Biomed Circuits Syst*, vol. 14, no. 5, pp. 971–984, Oct. 2020.

[3] D. Murzin *et al.*, “Ultrasensitive Magnetic Field Sensors for Biomedical Applications,” *Sensors*, vol. 20, no. 6, p. 1569, Mar. 2020.

[4] E. Elzenheimer *et al.*, “Quantitative Evaluation for Magnetoelectric Sensor Systems in Biomagnetic Diagnostics,” *Sensors*, vol. 22, no. 3, p. 1018, Jan. 2022.

[5] A. Kittmann *et al.*, “Wide Band Low Noise Love Wave Magnetic Field Sensor System,” *Scientific Reports*, vol. 8, no. 1, pp. 1–10, Jan. 2018.

[6] A. Kittmann *et al.*, “Sensitivity and noise analysis of SAW magnetic field sensors with varied magnetostrictive layer thicknesses,” *Sens Actuators A Phys*, vol. 311, p. 111998, Aug. 2020.

[7] P. Durdaut *et al.*, “Phase Noise of SAW Delay Line Magnetic Field Sensors,” *Sensors,* vol. 21, no. 16, p. 5631, Aug. 2021.

[8] J. M. Meyer *et al.*, “Thin-Film-Based SAW Magnetic Field Sensors,” *Sensors*, vol. 21, no. 24, p. 8166, Dec. 2021.

[9] S. Tamura, D. C. Hurley, and J. P. Wolfe, “Acoustic-phonon propagation in superlattices,” *Phys Rev B*, vol. 38, no. 2, p. 1427, Jul. 1988.

[10] V. Laude, M. Wilm, S. Benchabane, and A. Khelif, “Full band gap for surface acoustic waves in a piezoelectric phononic crystal,” *Phys Rev E Stat Nonlin Soft Matter Phys*, vol. 71, no. 3, p. 036607, Mar. 2005.

[11] S. Benchabane, A. Khelif, J. Y. Rauch, L. Robert, and V. Laude, “Evidence for complete surface wave band gap in a piezoelectric phononic crystal,” *Phys Rev E Stat Nonlin Soft Matter Phys*, vol. 73, no. 6, p. 065601, Jun. 2006.

[12] A. Khelif, B. Aoubiza, S. Mohammadi, A. Adibi, and V. Laude, “Complete band gaps in two-dimensional phononic crystal slabs,” *Phys Rev E Stat Nonlin Soft Matter Phys*, vol. 74, no. 4, p. 046610, Oct. 2006.

[13] A. Khelif and A. Adibi, “Phononic crystals: Fundamentals and applications,” *Phononic Crystals: Fundamentals and Applications*, pp. 1–245, Jul. 2015.

[14] M. Badreddine Assouar and M. Oudich, “Dispersion curves of surface acoustic waves in a two-dimensional phononic crystal,” *Appl Phys Lett*, vol. 99, no. 12, p. 123505, Sep. 2011.

[15] M. Oudich *et al.*, “Tailoring Structure-Borne Sound through Bandgap Engineering in Phononic Crystals and Metamaterials: A Comprehensive Review,” *Adv Funct Mater*, vol. 33, no. 2, p. 2206309, Jan. 2023.

[16] M. Samadi, J. Schmalz, J. M. Meyer, F. Lofink, and M. Gerken, “Phononic-Crystal-Based SAW Magnetic-Field Sensors,” *Micromachines*, vol. 14, no. 11, p. 2130, Nov. 2023.

[17] N. Kurz *et al.*, “Experimental determination of the electro-acoustic properties of thin film AlScN using surface acoustic wave resonators,” *J Appl Phys*, vol. 126, no. 7, p. 75106, Aug. 2019.

[18] C. Cordier and C. Dolabdjian, “Modeling of Delta-E Effect Magnetic Field Sensors,” *IEEE Sens J*, vol. 23, no. 3, pp. 2014–2020, Feb. 2023.

[19] J. Schmalz, E. Spetzler, J. McCord, and M. Gerken, “Investigation of Unwanted Oscillations of Electrically Modulated Magnetoelectric Cantilever Sensors,” *Sensors*, vol. 23, no. 11, p. 5012, May 2023.

[20] B. Spetzler, E. V. Golubeva, C. Müller, J. McCord, and F. Faupel, “Frequency Dependency of the Delta-E Effect and the Sensitivity of Delta-E Effect Magnetic Field Sensors,” *Sensors*, vol. 19, no. 21, p. 4769, Nov. 2019.